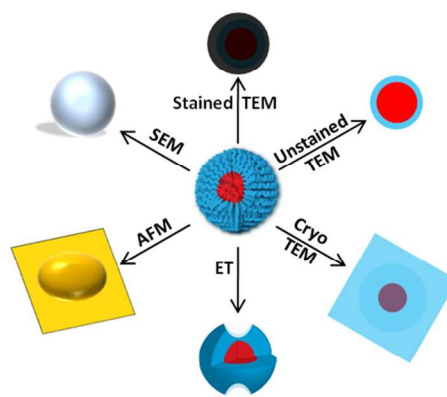
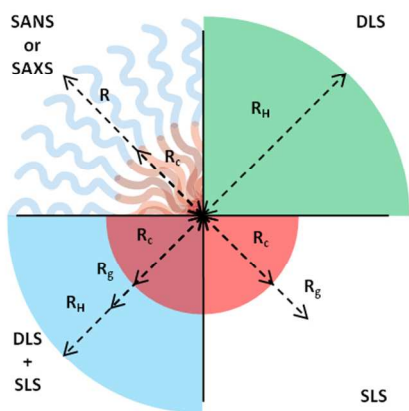




The analysis of solution self-assembled polymeric nanomaterials

Journal:	<i>Chemical Society Reviews</i>
Manuscript ID:	CS-REV-12-2013-060454.R1
Article Type:	Tutorial Review
Date Submitted by the Author:	30-Jan-2014
Complete List of Authors:	Patterson, Joseph; University of Warwick, Department of Chemistry Robin, Mathew; University of Warwick, Department of Chemistry Chassenieux, Christophe; LUNAM Université, Laboratoire Polymères, Colloïdes, Interfaces UMR CNRS 6120 Colombani, Olivier O'Reilly, Rachel; Warwick University, Department of Chemistry



Cite this: DOI: 10.1039/c0xx00000x

www.rsc.org/xxxxxx

ARTICLE TYPE

The analysis of solution self-assembled polymeric nanomaterials

Joseph P. Patterson,^a Mathew P. Robin,^a Christophe Chassenieux,^b Olivier Colombani^b and Rachel K. O'Reilly^{a,*}

Received (in XXX, XXX) Xth XXXXXXXXX 20XX, Accepted Xth XXXXXXXXX 20XX

DOI: 10.1039/b000000x

There has been much interest in the construction of soft nanomaterials in solution due to a desire to emulate the exquisite structure and function of Nature's equivalents (e.g. enzymes, viruses, proteins and DNA). Nature's soft nanomaterials are capable of selectivity, precision and efficiency in areas such as information storage and replication, transportation and delivery, and synthesis and catalysis. To this end, the use of small molecules, amphiphiles, colloids, and polymers have been investigated for the development of advanced materials in myriad fields of biomedicine and synthetic chemistry. Two major challenges are faced in this area of research: the reproducible, scalable and precise synthesis of such constructs and the reliable, accurate and in-depth analysis of these materials. This tutorial review will focus on this second aspect and provide a guide for the characterisation and analysis of soft nanomaterials in solution using scattering and microscopic techniques.

Introduction

The solution self-assembly of amphiphilic block copolymers (BCP)s provides access to a range of nanoscale structures, and research in this area has been given significant attention in relation to a variety of potential applications, including drug and gene delivery systems, nanoreactors, and in nanoelectronics.¹ Similar to small molecule amphiphiles, amphiphilic BCPs self-assemble into a variety of structures in solution, however, the macromolecular amphiphiles typically have much lower (or non-existent) critical micelle concentrations (CMC)s, greatly improved kinetic stability, and demonstrate ease of structure modification or functionalisation.² These favourable attributes, along with significant progress in controlled polymerisation techniques, have led to amphiphilic BCPs being extensively studied for applications that necessitate aqueous solution self-assembly.³

When discussing the self-assembly of small molecule amphiphiles, the final morphology can be predicted from the packing parameter 'p' related to the volume of the hydrophobic chains (v), the optimal area of the head group (a_0) and the length of the hydrophobic tail (l_c) by the equation $p = v / a_0 \cdot l_c$. In some cases, these thermodynamic considerations may be applied to BCPs self-assembly as well.⁴ However, determining the value of p is not straightforward for BCPs, especially when one of the blocks is a polyelectrolyte. Moreover, it is now well established that amphiphilic block copolymers usually form out of equilibrium or "frozen" structures^{5,6} especially in aqueous media where unimer exchange is almost impossible. As a result, the final morphology of the structures formed by BCPs is not only controlled by thermodynamic concepts such as the entropic

packing parameter, or enthalpic interactions, but is also strongly influenced by kinetic issues. In other words, the morphology of frozen assemblies of BCPs depends on the preparation pathway.⁵ As a result, while spheres, cylinders and polymersome morphologies tend to dominate the literature for diblock copolymers, other morphologies are possible such as bicontinuous structures⁷, toroids, discs, Janus, and multicompartamental aggregates.^{3,4}

While many of the standard analysis techniques available to chemists (e.g. NMR, IR, UV) can be used to infer information about polymer assemblies in solution, the most common techniques used to characterize their structure are based on microscopy and scattering. In the present paper, we tried to highlight what type of information scattering and microscopy techniques can bring and what are the key points to consider when relying on these techniques for polymeric nanomaterials formed in either water or organic solvents.

Analysis of polymers assemblies in solution

Scattering and microscopy techniques provide complementary information about the particles. Scattering techniques give good statistics (typically $> 10^9$ particles),⁸ and analysis can be conducted in solution with minimal effect on the sample. However, scattering data gives an overview of the sample and the data is often fitted to a model. This means that analysing samples containing multiple structures or completely unknown structures can be very problematic. Microscopy is complementary in that the sample can be imaged directly, allowing the differences in individual particles to be readily observed. However, analysis of

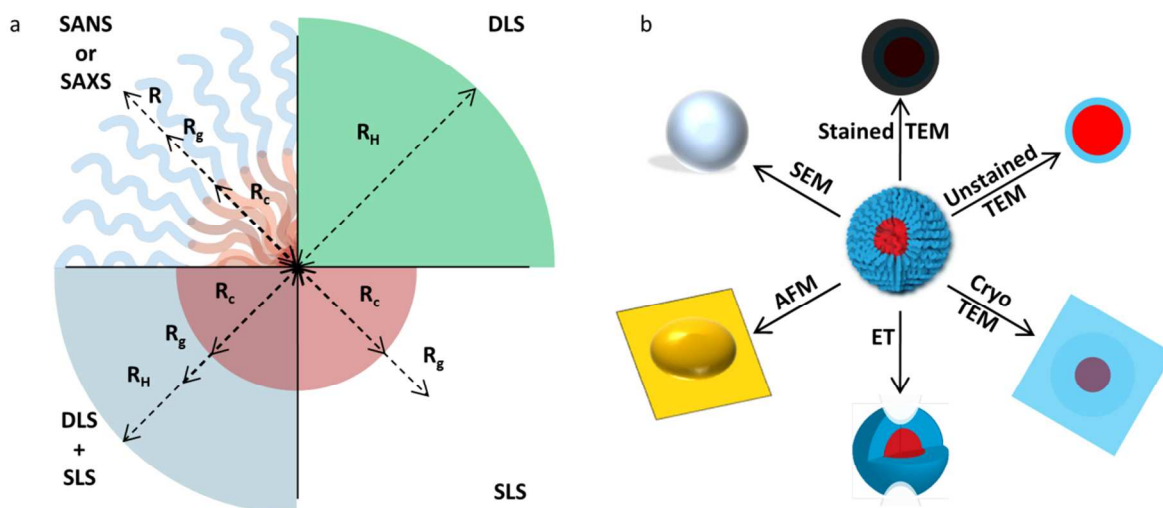


Fig. 1 A Schematic showing (a) the types of information which is obtainable by different scattering techniques and (b) the different types of images formed by different microscopy techniques for a spherical polymer micelle.

many particles can be time consuming which often results in extremely poor statistics. Moreover, microscopy is extremely subjective unless many different pictures of one sample are taken to make sure that the selected images are 'representative' of the sample and do not correspond to impurities or minor populations. Furthermore, almost all microscopy techniques involve removing the sample from its natural state in solution which can significantly alter its structure. Both the benefits and restrictions of analysis techniques should always be kept in mind to allow accurate characterisation of a sample and we have tried to highlight them in the following sections. However, this is by no means a complete list of the techniques available for analysing these systems, for example, Zeta potential, DOSY NMR, and nanoparticle tracking analysis (NTA) can provide useful information and more details of these techniques are included in the SI.

20 Scattering techniques for polymeric aggregates

The most common scattering techniques for soft materials in solution are static and dynamic light (SLS and DLS), small angle X-ray (SAXS) and small angle neutron scattering (SANS), see Figure 1. The basic principle in each case consists in illuminating the solution with a radiation of known wavelength and to detect the intensity scattered by the sample, at a given angle of observation with respect to the incident radiation. If the data are collected as a function of time, particle dynamics can be analysed as in the case of dynamic light scattering. On the contrary, averaging the scattered intensity over time scales much greater than those in which solution dynamics occur (for example 1000 x the relaxation time of the sample) results in scattering based on particle size and shape as for SLS, SANS and SAXS. Generally for strongly scattering systems (e.g. polymer micelles), the error in parameters obtained by DLS, SLS or SANS is roughly 10-20%,⁹ which can be attributed to the inaccuracies in radiation source, measuring the standards and sample parameters (see SI for more information). However, when comparing values from

the same apparatus under the same conditions, the errors can be considered to be significantly smaller and consequently an error of 5% can be applied.⁹

While there are many similarities between different scattering techniques, there are some important differences, which are primarily related to the wavelength of the incident radiation and to the way this radiation interacts with the particles (contrast). In all cases, as long as the contrast is sufficient, measurements will give information about the molecular weight, size and shape of the scatterers, and about the interactions between them. The length scale at which the matter is probed is inversely proportional to the scattering wave vector q (equation 1), larger q values thus corresponding to smaller length scales. The length scales being measured can be somewhat tailored by changing both the wavelength of the incident radiation (λ) and the scattering angle (θ). For light scattering n is the refractive index of the solution, whereas for SANS and SAXS $n = 1$ and is often omitted.

$$q = \frac{4\pi n}{\lambda} \sin\left(\frac{\theta}{2}\right) \quad (1)$$

Furthermore, since the contrast depends on the nature of the incident radiation, scatterers will be visualised differently depending on the technique, overall or more intimate structural characteristics can then be derived (fig. 1). In order to derive information about the molecular weight and size of individual particles, it is necessary to work in the dilute concentration regime. This ensures that only the particle form factor is measured, which relates to the interference of *intraparticle* scattering. Furthermore, even in this concentration range, in order to compute true values for the molecular weight and the size of the scatterers, measurements at different concentrations must be performed and extrapolation to zero concentration must be done. Otherwise, only apparent values (i.e. values at the measured concentration) can be derived, which are influenced by interactions between the scatterers. Scattering techniques can also

be used in the semi-dilute regime, but in this case the structure factor (the interference of *inter*particular scattering) of the scatterers is convoluted with their form factor giving access to information such as the correlation length and the existence of a local or higher length scale order of the particles rather than their size and molecular weight.

In the following, we will highlight the points one should be aware of when using scattering techniques. The reader is referred to more general references about DLS,¹⁰ SLS,¹¹ SAXS,¹² or SANS^{12,13} for more details.

Laser Light Scattering (LLS)

Dynamic Light Scattering (DLS)

Particles in solution move under Brownian motion and their diffusion coefficient D can be related to their (hydrodynamic) size by the Stokes-Einstein equation (equation 2).

$$R_H = \frac{k_B T}{6\pi\eta D} \quad (2)$$

Where k_B is Boltzmann's constant, T the absolute temperature and η the viscosity of the solvent. The consequence of this is that the hydrodynamic radius (R_H) reported by DLS is the theoretical radius of a perfect hard sphere which moves with the same translational diffusion coefficient (D) as the scatterers being measured. Therefore, the value of R_H is not equal to the radius of the particle, unless this particle is a hard sphere. Moreover, no morphology information can be extracted from a single DLS measurement.

In order to determine D it is necessary to measure the electric field and intensity auto-correlation functions, $g_1(q,t)$ and $g_2(q,t)$, which are respectively a measure of how quickly the electric-field and the scattered intensity change with time.¹⁰ For a perfectly monodisperse system, $g_1(q,t)$ can be modeled as a monoexponential decay which exhibits a single relaxation time τ . The apparent value of D measured at a given concentration (D_{app}) can then be computed from τ according to equation (3).

$$\tau^{-1} = D_{app} q^2 \quad (3)$$

For polymeric assemblies, which are never perfectly monodisperse, a cumulant is routinely applied. This assumes a monomodal distribution of relaxation times with a given dispersity. This routine is nevertheless not suitable for the multimodal distributions which are frequently observed with polymer nanomaterials. The CONTIN analysis is then preferred which fits the data with a constrained regularization method, and produces a continuous distribution of relaxation times, $A(\tau)$, and allows for the analysis of multiple broad distributions.⁸ Equation 3 can then be used to determine the diffusion coefficient (D) using the mean value of τ for any or all of the computed populations. Note that reliable values of τ can only be extracted if the auto-correlation functions are obtained with sufficient accuracy, i.e. good statistics and good signal/noise ratio. A rule of thumb is that the measurement time should be at least one thousand times as long as the largest τ value and the baseline for $g_2(t,q)$ should not be higher than 10^{-3} . R_H values from DLS are Z-averages, $\langle R_H \rangle_Z$. The weighting of larger structures in a Z-average can be seen from equation 4,

$$\langle R_H \rangle_Z = \frac{\sum c_i M_i R_i}{\sum c_i M_i} = \frac{\sum A_i R_i}{\sum A_i} \quad (4)$$

where, c_i is the weight concentration of scatterers of molecular weight M_i and radius R_i and where A_i is their relative scattering amplitude. This will be particularly important when comparing sizes obtained by different techniques (e.g. typically number averages are calculated for microscopy experiments). A few aspects should be kept in mind when performing DLS measurements. First, DLS measurements are very often performed using bench top apparatuses which are easy to use and provide a quick assessment of particle size distributions. However, one has to keep in mind that these setups usually operate at one or two angles (typically $\theta = 90^\circ$ and 173°). More sophisticated apparatuses allowing multi-angle measurements should be preferred whenever possible because they allow verification of the diffusive nature of particle displacement, i.e. that τ^{-1} is proportional to q^2 according to equation 3 and lead to a more accurate determination of D_{app} by plotting $\tau^{-1} \cdot q^{-2} = f(q^2)$ which should be a flat line corresponding to the value of D_{app} . Furthermore, the bench top instruments commonly provide intensity, volume and number size distributions for each measurement. The volume and number distributions are obtained from the intensity data by the assumption that $I \propto R^6$ and using equation 4. This manipulation of the measured intensity data can be useful to assess highly disperse or multimodal systems. However, it is important to remember that these conversions drastically emphasize information obtained from an extremely small fraction of the collected data (particularly in the case of the number distribution) and therefore R_H values obtained from these methods can be subject to significant errors.

Second, as pointed out above, data obtained at one concentration are only apparent values (D_{app} , $R_{H,app}$). In the dilute regime, D_{app} depends linearly on the concentration, C (equation 5). Measuring D_{app} for various concentrations will allow its extrapolation to zero concentration, so that the value of D_0 (and subsequently R_H with equation 2) which is not affected by interparticle interactions can be obtained. Extrapolation to zero concentration also yields k_D , the dynamic second virial coefficient, which depends both on the interactions between the particles (related to the static second virial coefficient A_2 , see next part SLS) and on the friction coefficient.¹⁰

$$D_{app} = D_0(1 + k_D \cdot C) \quad (5)$$

Third, it must be realized that the explanations given above remain valid only as long as multiple scattering does not occur; that is when each photon is only scattered once before being detected. To achieve such a condition the analyzed solutions must be perfectly transparent. Otherwise, the values of D and R_H obtained are incorrect. Dynamic light scattering of turbid solutions might be possible, but this requires the use of more sophisticated cross-correlation light scattering experiments.¹⁴ Fourth, it must be realized that the contribution to the scattered light is proportional to the molecular weight, contrast and concentration of the scatterers. The first parameter implies that the scattering of huge particles such as dust rapidly dominates the signal even if these particles are present in very small amounts. All solvents should then be filtered prior to measurements in order to remove dust. Solutions can also be filtered but one

should check that the filtration does not affect the sample morphology, size or concentration. It might be necessary to perform DLS and SLS simultaneously to take into account the contribution of a tiny amount of large spurious aggregates (see combining DLS and SLS section). For polyelectrolytes, light scattering experiments should be conducted in the presence of a molar excess of salt (e.g. NaCl) to prevent the so-called polyelectrolyte effect, which can lead to the apparition of slow modes (i.e. very large relaxation times).¹⁵

For spherical micelles R_H depends on the maximum chain length (L_{max}) of the BCP and the degree of polymer chain stretching (ω). L_{max} can be determined from the degree of polymerisation of both blocks ($N_{core + corona}$) and the monomer length (L_M), equation 6. For vinyl monomers $L_M = 0.25 \text{ nm}$.⁹ ω can then be determined by equation 7.

$$L_{max} = N_{core+corona} L_M \quad (6)$$

$$\omega = \frac{R_H}{L_{max}} \quad (7)$$

It is also possible to determine chain stretching by comparing R_H to the root mean square end-to-end distance (R_0) of the unperturbed polymer in dilute solution.¹⁶ This gives an indication of how confined or restricted the chains are within the aggregate. However, the ω values given by equation 7 are a clearer representation of whether or not the measured R_H values are realistic. For example, spherical micelles cannot have an ω value > 1 , as this would correspond to R_H greater than the maximum possible length of a constituent polymer chain.

Static Light Scattering (SLS)

The following discussion of SLS highlights some of the uses and limitations of this technique in relation to the analysis of polymeric assemblies. For a more detailed and general discussion the reader is directed to these texts.^{8, 10, 11}

As for DLS, SLS should be run with dust-free and fully transparent solutions (see above section). Contrary to DLS, SLS focuses on the mean value of the scattered intensity of a solution, which can be obtained by averaging the scattered light intensity measurements over time scales depending on the size of the scatterers in order to achieve good statistics, typically two or three repeats of each measurement should fall within 5% of each other. The Zimm equation (equation 8) is often used when performing SLS measurements at multiple angles (θ) and concentrations (c). The average scattered intensity of the sample (I_{sample}) is measured in relation to the average scattered intensity of the solvent ($I_{solvent}$) and a standard ($I_{standard}$). The Rayleigh ratio (R_θ) of the sample, which corresponds to the normalized contribution of the sample to the scattering intensity, is then determined based on the known Rayleigh ratio of the standard ($R_{\theta,standard}$), equation 9. Kc/R_θ can then be determined using equations 8-10 taking into account the wavelength of the laser (λ), the refractive index of the standard ($n_{standard}$), the refractive index increment (dn/dc) of the sample and Avogadro's number (N_A).

$$\frac{Kc}{R_\theta} = \frac{q^2 R_g^2}{3M_w} + \frac{1}{M_w} + 2A_2 c \quad (8)$$

$$R_\theta = \frac{I_{sample} - I_{solvent}}{I_{standard}} R_{\theta,standard} \quad (9)$$

$$K = \frac{4\pi^2 n_{standard}^2 \left(\frac{dn}{dc}\right)^2}{N_A \lambda^4} \quad (10)$$

The Zimm equation first implies that the Rayleigh ratio of the sample extrapolated to zero angle and zero concentration is proportional to the weight average molecular weight of the scatterers (M_w), to their concentration and to their contrast, the latter depending on the square of the refractive index increment (dn/dc). The dn/dc value must then be high enough (typically $> 0.08 \text{ mL/g}$) in order to be able to sufficiently dilute the sample. For block copolymers the dn/dc value should be determined directly with a differential refractometer. The Zimm plot treatment of the data is however subject to certain conditions, such that extrapolation of the data to zero angle and zero concentration is not always possible. First, the concentration must be sufficiently small so that only interactions between pairs of particles, represented by the term A_2 , exist. At higher concentrations, interactions between more than two particles may occur, causing a deviation of Kc/R_θ vs. c from linearity. Moreover, extrapolation of the data to zero concentration in order to get rid of the contribution of the interactions between the particles is only possible if their molecular weight does not change with concentration. This may be an issue if the self-assembled structures exhibit a high critical micellar concentration for example.¹⁷ Next, the Zimm approximation is only valid for small particles, that is for $qR_g < 1$ (typically $R_g < 80 \text{ nm}$), R_g being the radius of gyration of the particles. If these conditions are fulfilled, linear regression of Kc/R_θ vs. c yields the value of A_2 from the slope; which is negative for attractive interactions and positive for repulsive ones. Most polymer assemblies show positive A_2 values and for micelles these are on the order of 10^4 or $10^5 \text{ mL mol g}^{-2}$.¹⁸ Linear regression of Kc/R_θ vs q^2 yields the radius of gyration from the slope. R_g corresponds to the mean distance of one scattering centre within the particle, from the centre of the particle as a whole. However that accurate determination of R_g is only possible if the slope of this plot is sufficiently large. Particles with $R_g \leq 20 \text{ nm}$ will show roughly a 10% change in Kc/R_θ over the range of angles used, which is of the same order of magnitude as the typical error in SLS experiments, so that it is impossible to determine accurate values of $R_g \leq 20 \text{ nm}$. Finally, extrapolating Kc/R_θ to $q^2 = 0$ and $c = 0$ yields the molecular weight of the particles at the intercept. For polymer assemblies particle M_w is almost always used to determine the aggregation number (N_{agg}) of the assembly by equation 11.^{9, 18}

$$N_{agg} = \frac{M_{w,particle}}{M_{w,polymer}} \quad (11)$$

As the molecular weight obtained from SLS is a weight average molecular weight, it is more appropriate to use the weight average molecular weight of the polymer (M_w), rather than the number average (M_n). Note again, that if the data are only extrapolated to $q^2 = 0$ and not to $c = 0$, only an apparent molecular weight, M_{app} , will be obtained which is affected by interactions between the particles. Table 1 shows typical N_{agg} values for various BCPs and morphologies. The data shows that

Table 1. Summary of N_{agg} for various BCP assemblies

Polymer	Morphology	N_{agg}^a
PnBA- <i>b</i> -PAA ⁹	Spheres	100-500
PS- <i>b</i> -P4VP ¹⁶	Spheres	5-300
PS- <i>b</i> -Poly(L-lysine) ¹⁹	Cylinders	60-600
PEO- <i>b</i> -PCL ²⁰	Polymersomes	2,000-100,000

^a Measured by SLS

spheres can have a range of N_{agg} values from less than ten to a few hundred, for cylinders this will of course be related to the length and can either be in the range of spheres or much larger, while, for polymersomes N_{agg} values are typically very large.

Combining SLS and DLS

As discussed above, the scattered light intensity is proportional to the molecular weight and to the concentration of the scatterers. As a consequence, a very small concentration of very large scatterers (having a huge molecular weight) and a large concentration of small scatterers (with a small molecular weight) may contribute in similar amounts to the total scattered intensity although only the latter population of scatterers is representative of the sample. This situation arises frequently for polyelectrolyte solutions or for solutions containing micelles having a rather low aggregation number. Figure 2 shows typical DLS traces for polymeric assemblies, in this case hydrophobically modified poly(*N*-isopropylacrylamide) (PNIPAM) homopolymer micelles analysed in water. The data shows two populations for each sample, one smaller population, corresponding to the micelles, R_H ca. 20-40 nm (termed the fast mode of relaxation) and one larger population, R_H ca. 200-500 nm (termed the slow mode of relaxation). While the larger structures make a significant contribution to the overall scattering intensity, the larger aggregates can be considered to make up a negligible concentration in solution for the reason discussed above. This can be seen in the weight-averaged size distributions (Figure 2, inset), determined from the intensity data according to reference 18. In order to get rid of the contribution of the large spurious scatterers, both DLS and SLS should be performed simultaneously.¹⁸ The relative amplitude of the fast mode, A_{fast} , that is the percentage of the Rayleigh ratio coming from the contribution of the small scatterers, can be determined by DLS using the CONTIN routine.

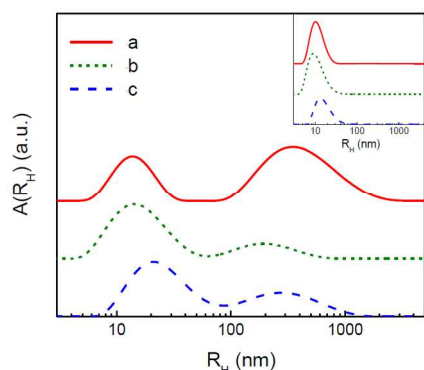


Fig. 2 Intensity weighted size distribution by DLS for three hydrophobically modified PNIPAM homopolymer micelles. Inset shows the weight-averaged size distributions.¹⁸

Table 2. R_g/R_H values and how they can be related to morphology

R_g/R_H^a	Equation	Topology	Morphology
0.775	$R_g^2 = 3/5 R^2$	Homogeneous sphere	Spherical micelles of R radius
1	$R_g^2 = \frac{3}{5} \left(\frac{R_o^5 - R_i^5}{R_o^3 - R_i^3} \right)$	Hollow sphere	Polymersomes with outer (R_o) and inner (R_i) radii
>1	$R_g^2 = L^2/12 + r^2/2$	Extended Structure	Cylinders of Length L and radius r

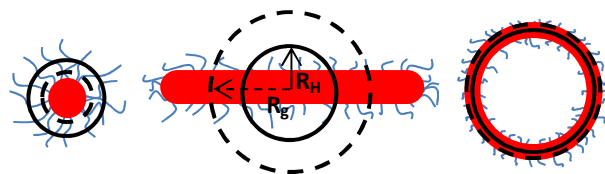
^aDetermined by a combination of DLS and SLS

Fig. 3 Schematic depicting how different morphologies would display a different R_g/R_H ratio where R_g is the radius indicated by the dashed black line and R_H is the radius indicated by the solid black line.

Then, the classical SLS treatment described in the previous part can be applied by replacing R_0 of the whole sample by $R_{0,\text{fast}} = A_{\text{fast}} R_0$ and using the total concentration c as the concentration of the small scatterers since the concentration of the large spurious scatterers can be considered negligible. DLS and SLS can also be combined to have an idea of the particle morphology as this is reflected by the ratio R_g/R_H , see Table 2 and Figure 3. The difference in R_g/R_H for spheres and polymersomes can be attributed to how the mass is distributed throughout the structures and for cylinders this is related to the fact they have reduced resistance when moving parallel to their extended axis.

Small Angle Neutron and X-ray Scattering (SANS and SAXS)

The following discussion of SANS and SAXS highlights some of the uses and limitations of these techniques in relation to the analysis of polymeric assemblies. For a more detailed and general discussion the reader is directed to these texts.^{12, 13}

One major problem with SANS and SAXS compared to LLS is the accessibility of the equipment. LLS experiments can be performed using equipment that is relatively cheap and can be contained on the bench top, whereas the majority of small angle measurements for carbon based samples in dilute solutions require more complex, high intensity radiation sources, e.g. reactors or particle accelerators. While commercially available SAXS equipment has been modified for this analysis (for example by Pedersen),²¹ this approach remains rare. However, in relation to light, both neutrons and X-rays have much smaller wavelengths (typically 0.1 nm) and consequently they can probe much smaller length scales (higher q values), giving information about the local structure of the assemblies including in particular shape and organization of the solvophobic and solvophilic blocks within the structure. Typical SANS and SAXS experiments start in a q -range where $q R_g < 1$, probing the whole of the scatterers, but go up to much larger q -values (smaller length scales) probing the interior of the scatterers ($q R_g > 1$).

One of the difficulty of SANS and SAXS is that quantitative interpretation of the scattering curves require their fitting with appropriate models. Pedersen and co-workers utilised SANS and

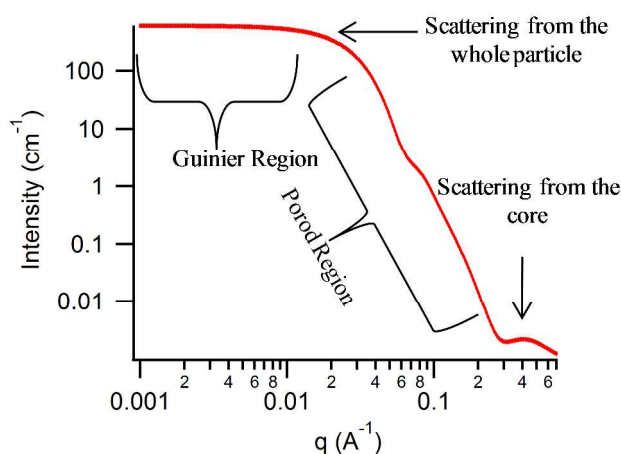


Fig. 4 a) SANS model showing I_s vs q for a disperse spherical particle with a core-shell structure. Model taken from reference.²⁴

SAXS to study spherical micelles of PS-*b*-poly(isoprene) (PS-*b*-PI) in decane.²² The models used to treat the data assumed a solid spherical core and a corona of semi flexible chains. They were able to determine not only aggregation numbers and micelle diameters, analogous to the information obtainable by LLS, but also information on the core size and corona profile (size and shape).²² Kelley and co-workers used a similar SANS model to determine the core size and corona profile for poly(1,2-butadiene-*b*-PEO) (PB-*b*-PEO) aggregates in various ratios of D₂O and THF-*d*₈.²³ They showed that with increasing THF content (good solvent for both blocks) both the core and corona size decreased while the concentration of unimers in solution increased (from effectively zero to about 50 %) resulting in a change from frozen to dynamic aggregates. Adams and co-workers utilised SAXS to study PEO-*b*-PCL polymersomes, and were able to measure the membrane thickness as a function of PCL block length.²⁰ One important limitation for SANS and SAXS quantitative treatment is that the models usually involve a large number of fitting parameters.^{12, 13} It is thus advisable to impose some of these parameters, obtained from other experiments (SLS, DLS, microscopy) to limit the number of free variables and converge into a realistic fit.

Finally, an important aspect of SANS and SAXS is the possibility to exploit contrast between different components of the system. Neutrons are scattered by the nucleus and the intensity of scattering is dependent on the nuclear scattering length density (SLD), determined for each sample from the chemical formula and density of the material.¹² Perhaps the most important consequence of the SLD is the significant difference observed between hydrogen and deuterium containing materials. This principle forms the basis of many SANS experiments for polymeric aggregates as deuterating polymers (see SI for more information) can be used to analyse scattering selectively from certain parts of the assembly for a more focused analysis.^{12, 13, 22} X-rays are scattered by the electron cloud and the intensity of scattering is proportional to atomic number squared (Z^2).¹² SAXS is therefore particularly sensitive to heavier elements, which allows enhancing the contrast of the corona of BCPs consisting of a polyelectrolyte hydrophilic block using heavier counter-ions. Figure 4 shows one example of a SANS model which is suitable for spherical micelles in order to demonstrate how some

information about the particles can be obtained. The Guinier region of the plot can give information about the overall size of the particle (as R increases the q value where the slope plateaus will decrease). Plotting $\ln(I_s)$ vs. q^2 for the points in this region (a Guinier plot) gives a linear fit where the gradient = $\frac{1}{2}R_g^2$. The Porod region corresponds to the scattering from local structure within the particle (i.e. morphology information). Plotting $\log(I_s)$ vs. $\log(q)$ should give a linear plot for this region where the gradient gives information about the morphology of the sample. Hollow structures will give a q^{-2} dependence whereas solid structures will show q^{-4} . Turning points at high q are indicative of scattering from smaller structures. For a core-shell particle (where the core and shell have sufficiently different SLDs) the q value for this 'hump' can give core radius (R) information by equation 12.

$$\frac{2\pi}{q} = 2R \quad (12)$$

Microscopy techniques for polymeric aggregates

The following discussion of microscopy techniques highlights some of the uses and limitations of this technique in relation to analysis of polymeric assemblies. For a more detailed discussion the reader is directed to these texts.²⁵⁻²⁹ Microscopy techniques complement scattering data as they directly image individual particles, typically when deposited onto a substrate or a support. Microscope types are numerous but can be broadly divided into three categories: optical, electron and scanning probe.²⁵ Optical and electron microscopes use a beam of radiation (e.g. light or electrons) which is projected onto the object in order to form an image of that object. Scanning microscopes use a probe which scans each point of the object serially in order to form an image of that object. The use of italics for 'an image' is meant as a reminder that an image is not the object itself, but merely a representation of the object, and furthermore, one object can be represented by many different types of images (Figure 1). The most common types of optical and electron microscopes are the light microscope and the transmission electron microscope (TEM), the latter of which is used extensively for the analysis of polymer assemblies and will be discussed in detail. Scanning microscopes are extremely numerous, but for those working with soft nanomaterials, scanning electron microscopy (SEM), scanning transmission electron microscopy (STEM) and atomic force microscopy (AFM) are the most commonly used. As STEM and SEM use electrons they can also be categorized as electron microscopes, however due to their imaging modes they are more appropriately categorized as scanning probe. The main differences in microscopy techniques come from a difference in how the image is formed. For example, images formed through transmission of radiation (e.g. TEM and STEM) show a projection of the entire structure, whereas many other types of microscopy (e.g. SEM and AFM), are only sensitive to surface (or near surface) structure and give an image which is more akin to that formed by the eye (Figure 1).²⁵ The absolute resolution (r) of an optical microscope can be determined using equation 13

$$r = \frac{0.61\lambda}{n \sin \alpha} \quad (13)$$

where λ is the wavelength of light, n is the refractive index of the

material and α is the angle formed between the object and the lens. Consequently resolution can be increased by decreasing λ or increasing n or $\sin \alpha$. In practice this limits the resolution of the light microscope ($\lambda = 200$ nm for UV-light microscopes) to about 150 nm and as such renders the technique of little use to those working on the nanoscale.²⁵ The major difference between light and electron microscopes is related to λ , which for electrons can be more than 100,000 times smaller, resulting in an absolute resolution of 0.003 nm (3.3 pm for 200 keV electrons). This is much smaller than the atomic radii of H (0.05 nm). While it is not quite possible to reach this resolution limit, due to aberrations caused by the electromagnetic lenses, imaging on the atomic scale for hard materials is routinely applied and even when using older, less advanced microscopes, researchers working on the nanoscale should not be concerned with the resolution limit of the microscope. The resolution for scanning microscopes varies from technique to technique, but generally they are either directly related to the size of the probe used, or to the degree in which a change in the probe (e.g. position or voltage) can be detected, the latter of which commonly results in atomic resolution.

Microscopy sample preparation dry state vs. solution state

Unlike the light microscope there are often difficulties associated with higher resolution techniques that make imaging in solution problematic. Therefore two general approaches exist for imaging polymer nanomaterials in solution. 1. Particles are dried onto substrates before imaging or 2. Special apparatus/techniques are used to keep the particles solvated while imaging. While the latter should be used whenever possible, these techniques are still not widely available / accessible and can limit imaging resolution. Therefore examples of dry state analysis are still prevalent in the literature and some considerations for these techniques will be discussed. It is well known that drying these samples can cause changes in particle size, morphology, crystallisation or even complete destruction of the particles.³⁰ Any solvated polymers in solution (e.g. micelle coronas) will completely change their shape upon dehydration. Polymers which are dehydrated in solution might be less affected, particularly those with a high T_g (e.g. a PS core at room temperature). Even for these nanoparticles which do survive the drying process, it must always be remembered that the measurements made (particle size, membrane thickness etc.) are those of the dried structures. The following sections detail both dry and solution state techniques and for the dry state techniques the previous considerations must always be kept in mind.

Transmission Electron Microscopy (TEM)

TEM is one of the most powerful methods for analysing nanomaterials. The extremely high spatial resolution is more than sufficient for anyone working on the nanoscale, and through transmission electron tomography,³¹ it is also possible to get 3D images and infer information about internal structure of the nanoparticle. Furthermore, with the use of analytical TEM techniques such as energy-filtered TEM (EFTEM), energy-dispersive x-ray spectroscopy (EDX) and electron energy loss spectroscopy (EELS),²⁵ it is now possible to chemically map out nanomaterials with atomic precision. TEMs operate with internal pressures of $< 10^{-10}$ Pa,²⁵ which is why dry state analysis is typically performed. This can be avoided by the use of cryo TEM

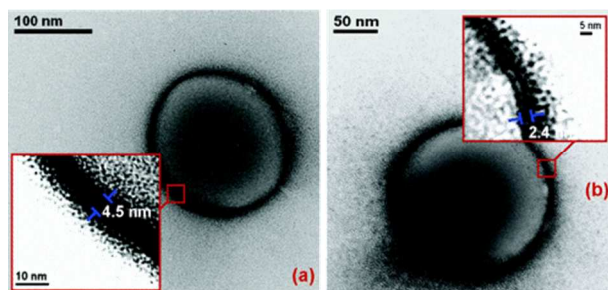


Fig. 5 Transmission electron micrograph of PEO₅₀-*b*-PBO₇₀ (a) and PEO₁₆-*b*-PBO₂₂ (b) polymersomes stained with uranyl acetate.³³

(discussed later) or more recently in situ flow cell TEM, which allows for the observation of particles in liquids at ambient temperatures.³² While the latter is an extremely exciting technique, allowing video capture of particle motion, there are currently very few publications regarding polymer nanoparticles and therefore this technique will not be discussed further.

Dry state TEM

The substrate to which the particles are dried is the source of another complication. Image contrast in TEM comes from either differences in the number of scattered electrons (termed mass-thickness or Z-contrast) or from changes to the phase of the electron waves (termed phase contrast). For mass-thickness contrast the number of electrons scattered depends on sample thickness and electron density (thicker or more electron dense materials will scatter more electrons). To observe particles easily the sample must scatter significantly more electrons than the support. Typical TEM grids consist of carbon based films which are roughly 40 nm thick, therefore, any carbon based sample approaching this size will be difficult to image on these grids. Although much thinner grids can be purchased (ca. 5 nm) their higher price and delicate nature often limits their use. Phase contrast mechanisms are much more complex than mass-thickness contrast, but essentially, by adjusting focus, phase contrast can be used to increase the contrast of the particles being imaged. Although phase contrast is used widely in cryo-TEM,³⁴ this approach is generally not sufficient to image carbon nanostructures on conventional TEM grids.

A more common approach has been to apply high atomic number stains (e.g. osmium tetroxide, ruthenium tetroxide, uranyl acetate, ammonium molybdate and phosphotungstic acid) which will selectively bind to the grid (negative staining) or the particle (positive staining), enhancing the contrast difference between them.²⁸ As scattering intensity is proportional to Z^2 , these stains appear extremely dark in comparison to either the support or the small carbon based particles. Figure 5 shows polymersomes formed from PEO-*b*-poly(1,2-butylene oxide) (PEO-*b*-PBO) stained with uranyl acetate.³³ One should be extremely cautious when using staining techniques as the scattering is dominated by the stain and not the particle. The images are actually a representation of what the stain adsorbs to, which is not necessarily a representation of the particles size, morphology or structure. Although uranyl acetate acted as a positive stain in this case, the nature of staining (positive or negative) will be dependent on the relative affinity for the polymer and the substrate. Generally speaking it has been shown that uranyl acetate interacts strongly with PAA, whereas osmium tetroxide

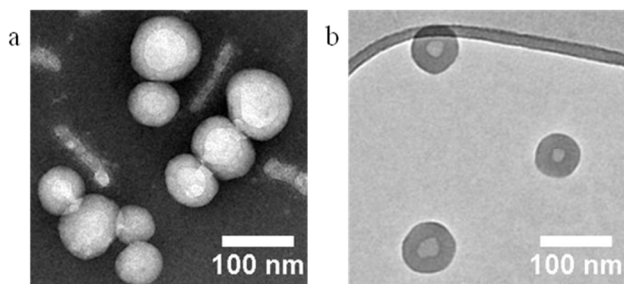


Fig. 6 PS₂₅₀-b-PAA₁₁ polymersomes imaged by (a) UA staining and (b) unstained on a GO-TEM grid.³⁷

and ruthenium tetroxide are known to interact with unsaturated bonds and aromatics.²⁸ However, these are only guides as to which stain might be an appropriate choice for the sample in question and not only must stains be selected with care (or screened) but the application of stain to the grid must also be optimised. While, the staining method has proven extremely useful, it has been well known for a long time that these stains can cause artefacts, limit resolution and obscure internal structure information.^{30, 34} With that in mind research has been conducted into creating the thinnest possible supports, so that smaller, more weakly scattering particles can be imaged without the need for staining. Graphene,³⁵ and graphene oxide (GO),³⁶ have been used as atomically thin sheets for imaging low contrast materials without staining. The hydrophilic nature of GO is particularly useful for adhering functional polymeric materials and polymer assemblies from both aqueous and organic solutions have been analysed by this method.³⁷ Figure 6 shows a comparison between a PS-b-PAA polymersome imaged by (a) dry state staining and (b) unstained on a GO-TEM grid. We recently showed that the same area of a GO-TEM grid can be imaged by TEM, AFM and SEM, which not only provides images from a series of complementary techniques but shows the robust nature of the support.³⁷ Imaging samples unstained should allow for atomic resolution to be achieved, however, polymeric assemblies, which are formed from low atomic number elements (typically C, H, N and O) can be considered weak phase objects. Therefore, they affect the phase of the electron wave more than its amplitude. Consequently in order to improve contrast, images are taken at large defocus values which limits the resolution for a single image. Dyson and co-workers recently showed exit wave reconstruction (EWR) in combination with GO-TEM grids can be used to overcome this resolution limit and as such produces extraordinary images where individual polymer chains can be observed within the nanostructures (Figure 7).³⁸

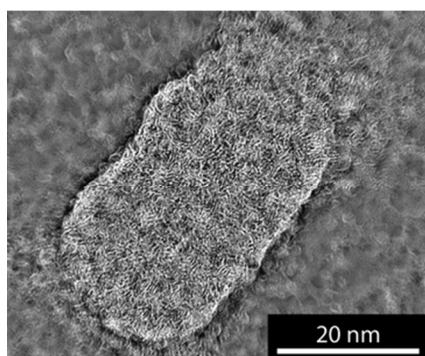


Fig. 7 EWR phase image for a poly(lactide)-b-PAA cylindrical micelle.³⁸

40 Cryo-TEM for polymeric aggregates

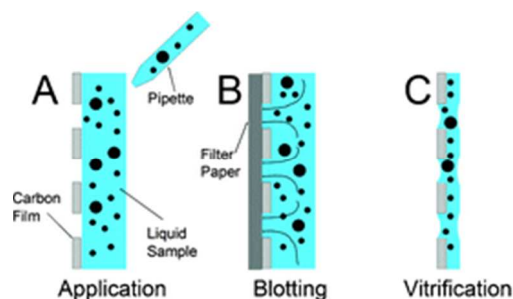


Fig. 8 Schematic of cryo-TEM sample preparation.³⁹

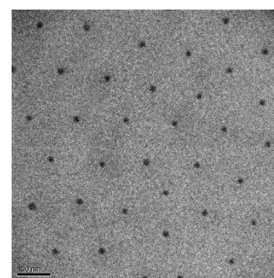


Fig. 9 Cryo-TEM of PnBA₉₀-b-PAA₃₀₀. Scale corresponds to 100 nm.⁹

Cryo-TEM is the most widely used method to avoid sample dehydration before imaging by TEM.³⁴ Figure 8 shows a schematic for the preparation of cryo-TEM grids. A small volume of sample solution (typically 3 μ L) is applied to a perforated TEM grid. The grid is blotted to remove almost all of the solution, creating a thin film (< 300 nm).³⁹ The grid is then rapidly plunged into a vitrification solvent (typically liquid ethane) in order to trap the sample in solution. Once vitrified, the grids are kept at liquid nitrogen temperatures during transfer to the microscope. This ensures that the sample remains vitrified and prevents evaporation or particle deformation while in the microscope. With this procedure it should be possible to get a snapshot of the particles in solution. As such, cryo-TEM has proven to be an extremely powerful technique for the analysis of polymer assemblies in solution. Indeed, Adams and co-workers utilised cryo-TEM to investigate the mechanism of polymersome formation. Samples were vitrified at different time points in order to capture the intermediate spherical and cylindrical morphologies.²⁰ Figure 9 shows a cryo-TEM image for the PnBA-b-PAA BCP micelles discussed in the LLS section. As the micelle corona (PAA in this case) remains hydrated, it is typically not visible in cryo-TEM and therefore the measured particle radii correspond to the radius of the core. The hexagonal arrangement is likely an artefact of the cryo-TEM preparation and it is interesting to note that the average distance between micelles (ca. 110 nm) is slightly larger than twice the size of the average corona length (ca. 47 nm). The disadvantages of cryo-TEM are typically associated with an increase in the time required to analyse samples and the increased cost and skills associated with grid preparation. The blotting and vitrification process mentioned above must take place in a 100 % humidity environment, to ensure that no evaporation will occur before vitrification (so that the sample is not concentrated and no cooling occurs).³⁴ This can be done manually or by the use of a controlled environment vitrification system (CEVS), which can be particularly useful as

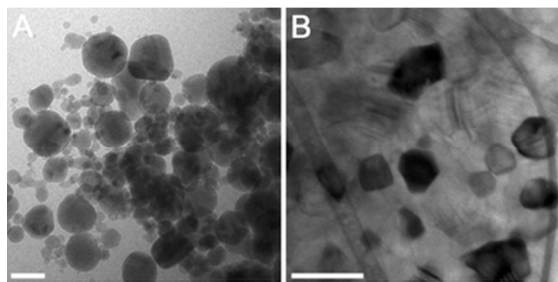


Fig. 10 Artifacts of different ice forms: (A) Large ice (frost) crystals; (B) hexagonal and truncated ice crystals. Some crystals seem extremely dark due to Bragg scattering of electrons. All scale bars represent 200 nm.³⁹

incorrect grid preparation can lead to a variety of artifacts.^{34, 39} For example, any exposure of the grid to air after vitrification (which is essentially unavoidable) will result in moisture from the air forming ice crystals on the cold surface of the grid. Figure 10 shows examples of these ice crystals, and demonstrates why this can be problematic while imaging, as they can obscure the view of the particles, and in some cases it can be hard to distinguish between ice and particles. Furthermore, when cryo-TEM samples are inserted into the microscope an appropriate amount of time must be left before imaging in order for the beam to stabilise due to temperature fluctuations. This typically limits the number of samples which can be analysed to about six per day for an experienced user. Extra care must also be taken when imaging as extended beam irradiation can damage both the ice and the particles, and consequently low dose techniques must be applied.³⁴ Another limitation for cryo-TEM, although rarely discussed, is the size limit for which particles can be detected. If the ice layer becomes too thin it will be both mechanically and electron beam unstable. Consequently there must be a size limitation for carbon based structures, where particles below this size are not observable due to the comparatively thick ice layer. This will be highly dependent on ice thickness and imaging parameters, but it is extremely difficult to observe particles where $R < 5$ nm. Furthermore, if the particles are too big, then they may be excluded from the grid during the preparation process and therefore particles $>$ ca. 300 nm will be difficult to analyse by cryo-TEM. One further limitation for cryo-TEM is that dedicated cryo-TEM instruments are often not equipped with the additional features that are routinely available on the modern TEM; for example scanning coils, which are used for imaging by STEM.

35 Scanning TEM (STEM) for polymeric aggregates

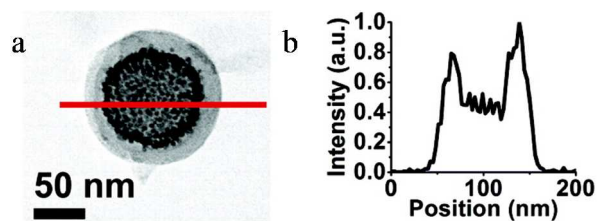


Fig. 11 (a) STEM image and (b) Fe intensity line scan generated from EDX for PS₁₉₈-*b*-PAA₃₈ magneto-core shell assemblies. Adapted from reference.⁴⁰

If a TEM is equipped with scanning coils, then these microscopes are usually called TEM/STEM microscopes. Instead of forming images by illuminating the object as a whole, in STEM mode

images are formed by a raster scan using a small beam of electrons. This analysis can be performed by either dry state or cryo-TEM. The spatial resolution in STEM is therefore directly related to the size of this electron beam and for modern STEMs this can be as low as 0.08 nm. The main advantage of STEM over TEM arises from its use as a “chemical analysis tool.”²⁵ Although STEM has excellent analysis capabilities, its use for assembled polymer systems has been scarce. Park and co-workers used STEM, EELS, and EDX to image Fe nanoparticles contained in PS-*b*-PAA assemblies in order to identify the location of the Fe nanoparticles within the structures (Figure 11).⁴⁰ EELS and EDX allow chemical compositions to be determined from specific areas within the images, which can be extremely useful in identifying the location of specific polymer blocks or encapsulated guests. Another benefit of STEM is the ability to image in the high angle annular dark field (HAADF) mode. This imaging mode is often referred to as mass-thickness contrast imaging as image contrast is directly related to the electron density and thickness of the specimen (i.e. no contribution from phase contrast). Consequently the images are more directly interpretable and more quantitative information can be obtained.^{27, 37} As they are performed in the same instrument, all the complications with sample preparation for TEM also apply to STEM, however, staining techniques are generally not used in conjunction with STEM as the benefits gained from the analytical tools are typically lost.²⁹ This makes the use of ultra-low contrast supports (e.g. graphene oxide) even more important for analysing materials in the dry state as the ability to use a wide range of techniques can be essential when identifying unknown structures. Recently a combination of TEM, EFTEM and HAADF-TEM has been used to prove the formation of hollow cylinders by a spontaneous one step drying induced reorganisation.⁴¹ One important limitation for all the TEM techniques discussed so far is that the images obtained are all 2D representation of 3D objects. In order to fully understand the 3D nature of the particles by TEM, electron tomography is required.

Electron Tomography (ET) for polymeric assemblies

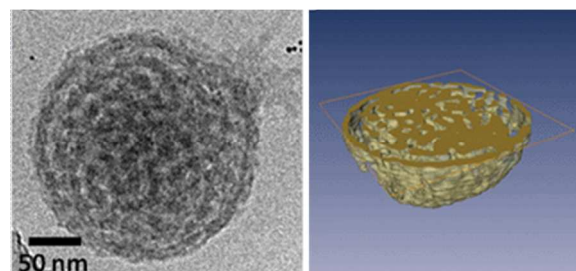


Fig. 12 (a) 2D cryoTEM image, (b) 3D reconstruction cross-section. Adapted from reference^{7, 31}

ET is a technique whereby a series of TEM images are recorded at various different tilt angles; this can be done either in the dry state or by cryo-TEM.^{31, 37} The images can then be reconstructed in order to obtain a 3D representation of the object under investigation.³¹ Figure 12 shows cryo-TEM images and 3D reconstructions for the bicontinuous structures analysed by Sommerdik and co-workers.⁷ The reconstruction was obtained by taking images from -70° to $+70^\circ$ in 1° increments. As such, ET requires a lot of images for a successful reconstruction and

therefore the electron dose applied to the specimen for each image must be sufficiently low so as not to damage the object or support over the extended imaging time. Due to the limitations of tilt angles available there is always some missing information in the reconstructions, often termed the ‘missing wedge’ (Figure 1),³¹ however, ET is still invaluable in the study of nanostructures with a complex internal structure as no other imaging technique can obtain such information for a single nanostructure. Unfortunately ET is not yet widely used to study assembled polymer systems which may be due to the difficulty or time consuming nature of the analysis compared to other imaging techniques which give 3D images, e.g. SEM and AFM.

Scanning Electron Microscopy for polymeric assemblies

SEM images are formed by raster scan using a small beam of electrons (similar to STEM), however, the electrons generally have much lower energies (typically 1 - 30 keV) than those used for TEM or STEM (typically 100 – 300 keV). The beam sizes are typically much larger than those in STEM and therefore the spatial resolution is limited to about 5 nm.²⁵ This low resolution in comparison to TEM / STEM is probably the main reason why SEM has been less widely used for the characterisation of polymer nanostructures. SEM is however, complementary to TEM / STEM in that the electrons are collected by a back scatter detector (i.e. not transmission). Therefore rather than giving internal structure information (as in TEM / STEM), the images provide surface (or near surface) information on the particles. SEMs are normally equipped with EDX detectors allowing for chemical analysis of the surface.²⁵ SEM instruments also operate under a vacuum, and the same sample preparation considerations that were discussed for TEM apply to SEM. Typically, carbon based samples are coated with a conducting material (e.g. Au or Pt), which helps to avoid build-up of charge on the sample, preventing image distortion.²⁵ Figure 13 shows an SEM image of PS-*b*-polyisocyanalanine(2-thiophene-3-yl-ethyl)amide (PS-*b*-PIAT) polymersomes which shows that the internal membrane is not visible due to the surface sensitive nature of SEM. However, it is common for polymersomes to ‘burst’ (as indicated by the blue circles in Figure 13) during sample preparation which can reveal holes in the structures, and is often seen as evidence of a hollow interior.⁴² While SEM images can give 3D information, they cannot accurately determine the height or topology of small particles, for which AFM is a more suitable technique.

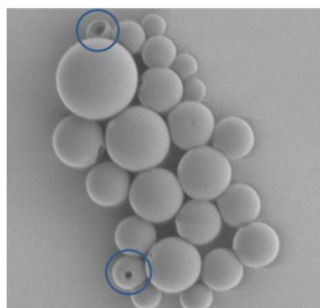


Fig. 13 SEM image of PS-*b*-PIAT polymersomes.⁴²

Atomic Force Microscopy for polymeric aggregates

AFM images are formed by dragging or tapping a sharp tip across the surface of the sample and, similar to SEM, can provide

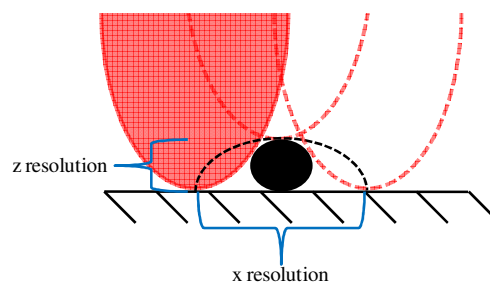


Fig. 14 Schematic of an AFM tip measuring a particle on the surface, indicating how the X resolution is limited due to tip convolution effects.

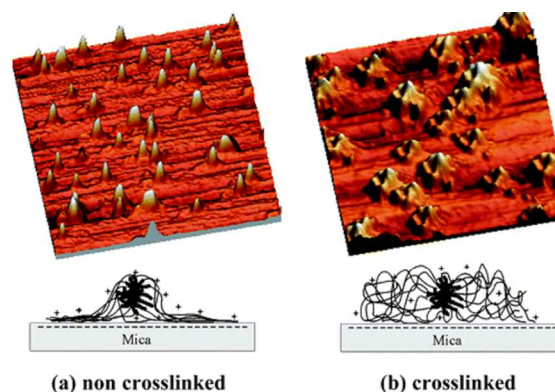


Fig. 15 AFM topography image of PL₄₉-b-PLYS₁₇₈ micelles adsorbed on mica surfaces and performed in an acid polymer solution. (a) Noncross-linked micelles. (b) Cross-linked micelles.⁴⁴

information about the particle surface.⁴³ Figure 14 shows how the x resolution in AFM is limited by the size of the tip due to convolution effects, which are generally on the order of 5-10 nm.²⁶ However, AFM resolution in the z direction is extremely high and most AFMs are easily capable of atomic resolution.²⁶ This feature has made AFM analysis of extremely small particles, or particles which give weak scattering in TEM, very appealing. Scherman and co-workers used AFM to image single chain nanoparticles formed from 168 kDa poly(N-hydroxyethylacrylamide) (PHEAm).⁴⁵ The particles were analysed by DLS in water which gave R_H values of 19 nm, indicating that they are hydrated in water and therefore would probably not be visible by cryo-TEM. Once dried to the surface of the AFM substrate (mica) they are extremely flat (a few nm) which would probably make them difficult to image by TEM in the dry-state. Although more beneficial for smaller particles, AFM has still proven useful in identifying the 3D nature of larger polymer structures when dried to a surface.⁴⁶ Again the drying effects discussed for TEM must also be considered here. However, for AFM it is also possible to image structures while hydrated through the use of liquid AFM. Lecommandoux and co-workers imaged PI-*b*-poly(L-lysine) (PI-*b*-PLys) micelles in an aqueous environment adsorbed to a mica surface by AFM and could distinguish between the cross-linked and non-crosslinked particles (Figure 15).⁴⁴ AFM of solutions has proven extremely useful in the biological sciences and is therefore often termed biological AFM. However, as AFM is only surface sensitive, measurements can only be made for particles that are surface active (i.e. not in the bulk), which limits its use for polymer aggregates in solution.

The power of complementary analysis

Several examples have been used throughout this review not only because they effectively demonstrate what information can be obtained by the various analysis techniques, but also because they demonstrate the power and confidence gained when using multiple techniques to verify and correlate results.^{9, 18, 20, 23, 37} The ratio R_g/R_H obtained by combining DLS and SLS gives an idea of the polymer morphology, which is not possible through either individual technique. This information can then be compared to morphology information determined directly by SANS and SAXS or directly observed by cryo-TEM. M_w values are not often derived from SANS/SAXS/cryo-TEM experiments. However, for spherical morphologies, it is possible to deduce the aggregation number N_{agg} from the size of the core (R_{core}) through equation 14, assuming the core block is completely dehydrated and its density is equal to its bulk density ρ_{core} .^{9, 47} This value can be compared to the N_{agg} determined by SLS.

$$\frac{4\pi\rho R_{core}^3}{3} = N_{agg} \frac{MW_{core\ block}}{N_A} \quad (14)$$

It should also be pointed out that large variations of the aggregation number are not always accompanied by significant variation of the size of the particle. This is particularly true for star-shaped micelles formed by neutral BCPs where the hydrodynamic radius scales only with $N_{agg}^{0.2}$.⁴⁸ For this reason, it is really worth measuring not only the morphology and size of BCPs assemblies but also their molecular weight (or aggregation number).

On top of that, new information can be derived from the combination of different techniques. For example, for core-shell spherical particles, the thickness of the corona can be estimated by subtracting the radius of the core to the hydrodynamic radius of the particles (equation 15).

$$R_{corona} = R_H - R_{core} \quad (15)$$

Colombani and co-workers used this approach for PnBA-*b*-PAA frozen micelles. This allowed for a direct examination of the change in stretching of the PAA corona with changes in ionisation and salt concentrations.⁹ When trying to verify a certain feature of the nanostructure (e.g. size and morphology) combining techniques which can directly visualise the particles (microscopy) with techniques that give an overview of large

numbers of particles (scattering) ensures a robust conclusion can be drawn (Table 3). Two recent examples of this have been the correlation of radial profiles obtained from cryo-TEM with those obtained by SANS,¹⁸ and SAXS.⁴⁹ These reports show that detailed and quantitative information can be extracted from cryo-TEM micrographs and highlight the immense potential for the use of these complimentary techniques.

Additionally, being able to characterize the assemblies formed by BCPs in solution can be used to probe the exchange dynamics in these systems, that is the rate at which hydrophobic blocks exchange between different cores, as highlighted in ref.⁶ First, it is clear that if the characteristics of the assemblies depend on the preparation pathway, these structures are “frozen”, that is out of equilibrium and unable to exchange unimers within the observation time scale.⁵ More quantitatively, assemblies able to exchange unimers should rearrange upon variation of external stimuli affecting their equilibrium structure. The rate at which this occurs is an indication of the exchange dynamics. Finally, time resolved small angle scattering techniques have been shown to be a very powerful method to study the exchange dynamics in self-assembled BCPs structures at steady state.⁵⁰

Conclusions

Although there are many applications for which the self-assembly of polymers in solution could provide utility, and while there is a vast range of synthetic and analytical techniques available, there is a long way to go before many of these applications are realised. Generally, the analysis of polymer aggregates seeks to answer two basic questions: What is their size? And what is their morphology? But why stop there? Why not ask how each polymer chain is positioned within the assembly? What about the position of each individual atom? The latter of these is clearly beyond our current analysis capabilities, although recent advances may provide new opportunities for such improvements. While there is a long way to go before the characterisation of polymer aggregates in solution becomes as thorough and readily accessible as that of the polymers themselves (or even small molecules), many exciting advances continue to be presented in the literature and with the appropriate use of well performed analysis a detailed understanding of the nanostructures in solution can be obtained.

Table 3. Summary of the information which is routinely available for each analysis technique

Technique	Size ^a	Morphology ^b	Internal structure ^b	3D structure ^b	Molecular weight ^b
DLS	R_H	X	X	X	X
MA-DLS	R_H	*	X	*	X
SLS	R_g	*	X	*	✓
MA-DLS + SLS	$R_H + R_g$	✓	✓	✓	✓
SANS	R_c, R_g, R	✓	✓	✓	✓
SAXS	R_c, R_g, R	✓	✓	✓	✓
Stained TEM ^c	R	*	X	X	X
Unstained TEM ^c	R	✓	✓	X	X
Cryo-TEM	R_c, R	✓	✓	X	*
ET (cryo/unstained ^c)	R_c, R	✓	✓	✓	*
AFM ^c	Height	✓	X	✓	X
SEM ^c	R	✓	*	X	X

^aWhich type of size is determined, ^bthe information is either, directly measured (✓), inferred through interpretation or further calculation (*) or is not obtainable (X), ^ccorresponding to the radius of the dried structures

Notes and references

^a Department of Chemistry, University of Warwick, Gibbet Hill Road, Coventry, CV4 7AL, United Kingdom; E-mail: r.k.o-reilly@warwick.ac.uk

^b LUNAM Université, Université du Maine, IMMM UMR CNRS 6283, PCI Department, Avenue Olivier Messiaen, 72085 Le Mans Cedex 09, France

† Electronic Supplementary Information (ESI) available: Contains additional information and references for the various techniques discussed. See DOI: 10.1039/b000000x/

1. G. L. M. Lazzari, S. Lecommandoux, *Block Copolymers in Nanoscience*, Wiley-VCH, 2006.
2. R. K. O'Reilly, M. J. Joralemon, K. L. Wooley and C. J. Hawker, *Chem. Mater.*, 2005, **17**, 5976-5988.
3. Y. Mai and A. Eisenberg, *Chem. Soc. Rev.*, 2012, **41**, 5969-5985.
4. A. Blanazs, S. P. Armes and A. J. Ryan, *Macromolecular Rapid Communications*, 2009, **30**, 267-277.
5. R. C. Hayward and D. J. Pochan, *Macromolecules*, 2010, **43**, 3577-3584.
6. T. Nicolai, O. Colombani and C. Chassenieux, *Soft Matter*, 2010, **6**, 3111-3118.
7. A. L. Parry, P. H. H. Bomans, S. J. Holder, N. A. J. M. Sommerdijk and S. C. G. Biagini, *Angew. Chem., Int. Ed.*, 2008, **47**, 8859-8862.
8. W. Schärfl, *Light scattering from polymer solutions and nanoparticle dispersions*, Springer Berlin, 2007.
9. O. Colombani, M. Ruppel, M. Burkhardt, M. Drechsler, M. Schumacher, M. Gradzielski, R. Schweins and A. H. E. Müller, *Macromolecules*, 2007, **40**, 4351-4362.
10. W. Brown, *Dynamic light scattering: the method and some applications*, Oxford University Press, USA, 1993.
11. W. Brown, *Light scattering: principles and development*, Clarendon Press Oxford, 1996.
12. R.-J. Roe and R. Roe, *Methods of X-ray and neutron scattering in polymer science*, Oxford University Press New York, 2000.
13. J. S. Higgins and H. Benoît, *Polymers and neutron scattering*, Clarendon Press Oxford, 1994.
14. C. Urban and P. Schurtenberger, *J. Colloid Interface Sci.*, 1998, **207**, 150-158.
15. H. Dautzenberg, W. Jaeger, J. Kötz, B. Philipp, C. Seidel and D. Stscherbina, *Polyelectrolytes: formation, characterization and application*, Hanser Munich, Munich, Vienna, New York, 1994.
16. S. Forster, M. Zisenis, E. Wenz and M. Antonietti, *J. Chem. Phys.*, 1996, **104**, 9956-9970.
17. C. Charbonneau, M. M. De Souza Lima, C. Chassenieux, O. Colombani and T. Nicolai, *PCCP*, 2013, **15**, 3955-3964.
18. J. P. Patterson, E. G. Kelley, R. P. Murphy, A. O. Moughton, M. P. Robin, A. Lu, O. Colombani, C. Chassenieux, D. Cheung, M. O. Sullivan, T. H. Epps and R. K. O'Reilly, *Macromolecules*, 2013, **46**, 6319-6325.
19. A. Lübbert, V. Castelletto, I. W. Hamley, H. Nuhn, M. Scholl, L. Bourdillon, C. Wandrey and H.-A. Klok, *Langmuir*, 2005, **21**, 6582-6589.
20. D. J. Adams, C. Kitchen, S. Adams, S. Fuzeland, D. Atkins, P. Schuetz, C. M. Fernyhough, N. Tzokova, A. J. Ryan and M. F. Butler, *Soft Matter*, 2009, **5**, 3086-3096.
21. J. Pedersen, *J. Appl. Crystallogr.*, 2004, **37**, 369-380.
22. J. S. Pedersen, I. W. Hamley, C. Y. Ryu and T. P. Lodge, *Macromolecules*, 2000, **33**, 542-550.
23. E. G. Kelley, T. P. Smart, A. J. Jackson, M. O. Sullivan and T. H. Epps, *Soft Matter*, 2011, **7**, 7094-7102.
24. V. Degiorgio and M. Corti, *Physics Of Amphiphiles: Micelles, Vesicles And Microemulsions: Proceedings Of The International School Of Physics*, Elsevier Science Ltd, 1985.
25. P. J. Goodhew, F. J. Humphreys and R. Beanland, *Electron microscopy and analysis*, Taylor & Francis Group, 2001.
26. F. J. Giessibl, *Rev. Mod. Phys.*, 2003, **75**, 949-983.
27. J. Loos, E. Sourty, K. B. Lu, G. de With and S. van Bavel, *Macromolecules*, 2009, **42**, 2581-2586.
28. M. R. Libera and R. F. Egerton, *Polym. Rev.*, 2010, **50**, 321-339.
29. A. A. Sousa and R. D. Leapman, *Ultramicroscopy*, 2012, **123**, 38-49.
30. Y. Talmon, *J. Colloid Interface Sci.*, 1983, **93**, 366-382.
31. F. Nudelman, G. de With and N. A. J. M. Sommerdijk, *Soft Matter*, 2011, **7**, 17-24.
32. M. T. Proetto, A. M. Rush, M.-P. Chien, P. Abellan Baeza, J. P. Patterson, M. P. Thompson, N. H. Olson, C. E. Moore, A. L. Rheingold, C. Andolina, J. Millstone, S. B. Howell, N. D. Browning, J. E. Evans and N. C. Gianneschi, *Journal of the American Chemical Society*, 2014, DOI: 10.1021/ja408513m.
33. G. Battaglia and A. J. Ryan, *J. Am. Chem. Soc.*, 2005, **127**, 8757-8764.
34. H. Friedrich, P. M. Frederik, G. de With and N. A. J. M. Sommerdijk, *Angew. Chem., Int. Ed.*, 2010, **49**, 7850-7858.
35. J. C. Meyer, C. O. Girit, M. F. Crommie and A. Zettl, *Nature*, 2008, **454**, 319-322.
36. N. R. Wilson, P. A. Pandey, R. Beanland, R. J. Young, I. A. Kinloch, L. Gong, Z. Liu, K. Suenaga, J. P. Rourke, S. J. York and J. Sloan, *ACS Nano*, 2009, **3**, 2547-2556.
37. J. P. Patterson, A. M. Sanchez, N. Petzetakis, T. P. Smart, I. I. T. H. Epps, I. Portman, N. R. Wilson and R. K. O'Reilly, *Soft Matter*, 2012, **8**, 3322-3328.
38. M. A. Dyson, A. M. Sanchez, J. P. Patterson, R. K. O'Reilly, J. Sloan and N. R. Wilson, *Soft Matter*, 2013, **9**, 3741-3749.
39. H. Cui, T. K. Hodgdon, E. W. Kaler, L. Abezgauz, D. Danino, M. Lubovsky, Y. Talmon and D. J. Pochan, *Soft Matter*, 2007, **3**, 945-955.
40. R. J. Hickey, A. S. Haynes, J. M. Kikkawa and S.-J. Park, *J. Am. Chem. Soc.*, 2011, **133**, 1517-1525.
41. N. Petzetakis, M. P. Robin, J. P. Patterson, E. G. Kelley, P. Cotanda, P. H. H. Bomans, N. A. J. M. Sommerdijk, A. P. Dove, T. H. Epps, III and R. K. O'Reilly, *ACS Nano*, 2013, **7**, 1120-1128.
42. D. M. Vriezema, J. Hoogboom, K. Velonia, K. Takazawa, P. C. M. Christianen, J. C. Maan, A. E. Rowan and R. J. M. Nolte, *Angew. Chem., Int. Ed.*, 2003, **42**, 772-776.
43. P. Eaton and P. West, *Atomic Force Microscopy*, OUP Oxford, 2010.
44. J. Rodríguez-Hernández, J. Babin, B. Zappone and S. Lecommandoux, *Biomacromolecules*, 2005, **6**, 2213-2220.
45. E. A. Appel, J. d. Barrio, J. Dyson, L. Isaacs and O. A. Scherman, *Chem. Sci.*, 2012, **3**, 2278-2281.
46. A. Presa Soto, J. B. Gilroy, M. A. Winnik and I. Manners, *Angew. Chem., Int. Ed.*, 2010, **49**, 8220-8223.
47. C. Burguiere, C. Chassenieux and B. Charleux, *Polymer*, 2002, **44**, 509-518.
48. M. Daoud and J. P. Cotton, *J. Phys. (Les Ulis, Fr.)*, 1982, **43**, 531-538.
49. J. J. Crassous, C. N. Rochette, A. Wittemann, M. Schrunner, M. Ballauff and M. Drechsler, *Langmuir*, 2009, **25**, 7862-7871.
50. R. Lund, L. Willner and D. Richter, in *Controlled Polymerization and Polymeric Structures*, eds. A. Abe, K.-S. Lee, L. Leibler and S. Kobayashi, Springer International Publishing, 2013, vol. 259, pp. 51-158.

Biographies



Joseph Patterson graduated from the University of York with a 1st class Master's degree in chemistry in 2009. He went on to complete his PhD under the supervision of Rachel O'Reilly at the University of Warwick where he won the Domino MacroGroupUK young polymer award at the Young Researchers Meeting in 2011. He is currently working for Nathan Gianneschi as a postdoctoral scholar at the University of California San Diego. His research interests include the analysis of soft nanomaterials in solution through the use of multiple complementary techniques, the development of electron microscopy methods and the self-assembly of amphiphilic block copolymers.



Mathew Robin was born in Jersey, Channel Islands, and graduated from Jesus College, University of Cambridge with a first class BA in Natural Sciences in 2009. He then completed an MSc in Chemistry at the University of Kent, under the supervision of Dr Simon J. Holder. He is currently in the final year of his PhD at the University of Warwick, under the supervision of Prof. Rachel K. O'Reilly. His research focuses on the self-assembly of polymers in solution, and the synthesis of fluorescent polymers and nanomaterials.



Olivier Colombani received a PhD in polymer chemistry from the University Pierre et Marie Curie in Paris in 2003. After two post-doctoral positions, respectively at the University of Bayreuth in Germany and at the Centre of Nuclear Energy (CEA) in France, he was employed as assistant professor at the University of Le Mans in 2006. He currently focuses on self-assembling polymers in solution, aiming at directing their organization, exchange dynamics and resulting macroscopic properties through the control of their chemical structure.



Christophe Chassenieux has been hired as a Professor by the University of le Mans in 2005 after being an assistant professor at Université Pierre et Marie Curie - Paris during 7 years. He received his PhD in polymer science in 1997 and then joined the group of Pr. M. A. Winnik in Toronto as a postdoctoral fellow for one year. His current research topics deal with the design, the characterisation and the use of polymeric self-assemblies based on amphiphilic copolymers as building blocks for designing smart hydrogels. He is the co-author of fifty research papers, 4 patents and he has co-edited two books.



Rachel O'Reilly is currently a professor and an ERC consolidator grant awardee in the Chemistry Department at the University of Warwick. She started in independent career in 2005 with the award of a Royal Society Dorothy Hodgkin Fellowship at the University of Cambridge. In 2009 she moved to Warwick with the award of an EPSRC career acceleration fellowship and in 2012 was promoted to full professor. In 2012 she won the IUPAC-Samsung young polymer scientist award and the RSC Hickinbottom medal. In 2013 she was awarded the ACS Mark Young Scholar award and was elected as an ACS POLY fellow. Her research focuses on bridging the interface between creative synthetic, polymer and catalysis chemistry, to allow for the development of materials that are of significant importance in medical, materials and nanoscience applications.

Key learning objectives

- 1) What information should we seek to obtain about polymer assemblies in solution?
- 2) What are the main analysis techniques used for nanoscale polymer assemblies?
- 3) Why is it important to use a combination of different techniques?
- 4) What are the main strengths and weaknesses associated with each technique?